J|A|C|S

JOURNAL OF THE AMERICAN CHEMICAL SOCIETY

Article

pubs.acs.org/JACS

# Enhanced Stability and CO/Formate Selectivity of Plasma-Treated SnOx/AgOx Catalysts during CO2 Electroreduction

Yong-Wook Choi,[†] Fabian Scholten,[†,‡] Ilya Sinev,[†] and Beatriz Roldan Cuenya*,[†,‡]

[†]Department of Physics, Ruhr University Bochum, 44780 Bochum, Germany

[‡]Department of Interface Science, Fritz-Haber Institute of the Max Planck Society, 14195 Berlin, Germany

S *Supporting Information*

ABSTRACT: CO_2 electroreduction into useful chemicals and fuels is a promising technology that might be used to minimize the impact that the increasing industrial CO_2 emissions are having on the environment. Although plasma-oxidized silver surfaces were found to display a considerably decreased overpotential for the production of CO, the hydrogen evolution reaction (HER), a competing reaction against CO_2 reduction, was found to increase over time. More stable and C1-product-selective SnO_x/AgO_x catalysts were obtained by electrodepositing Sn on O_2-plasma-pretreated Ag surfaces. In particular, a strong suppression of HER (below 5% Faradaic efficiency (FE) at −0.8 V vs the reversible hydrogen electrode, RHE) during 20 h was observed. *Ex situ* scanning electron microscopy (SEM) combined with energy-dispersive X-ray spectroscopy (EDS), quasi *in situ* X-ray photoelectron spectroscopy (XPS), and *operando* X-ray absorption near-edge structure spectroscopy (XANES) measurements showed that our synthesis led to a highly roughened surface containing stable $Sn^{\delta+}/Sn$ species that were found to be key in the enhanced activity and stable CO/formate ($HCOO^-$) selectivity. Our study highlights the importance of roughness, composition, and chemical state effects in CO_2 electrocatalysis.
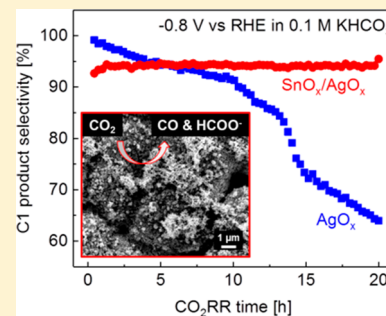
1. INTRODUCTION

More efficient processes for the electrochemical CO_2 reduction (CO_2RR) are currently actively sought in order to mitigate the negative effects associated with the increased CO_2 in our atmosphere such as in global warming while producing valuable chemicals and fuels (CH_4, C_2H_4, C_2H_5OH, etc.). Additional products from CO_2RR such as CO and formate, for which higher selectivity at lower overpotentials can be achieved, have been discussed to be economically more feasible than some hydrocarbon and alcohol products. This is based in the current price of grid electricity and the cost of CO_2 capture for CO_2RR if it is not already available in a concentrated form at an industrial site.[1]

It is well known that p-block metal catalysts such as tin (Sn), lead (Pb), indium (In), and thallium (Tl) can mainly produce $HCOO^-$ during CO_2RR, while CO can be primarily obtained over gold (Au), silver (Ag), and zinc (Zn) catalysts.[2] Although Au has displayed remarkable catalytic activity and a high Faraday efficiency (FE) for CO at a low overpotential (87% at −0.74 V vs the reversible hydrogen electrode, RHE[3]), recent studies have tried to find alternative catalysts owing to the high price of Au.[4−6] Nonprecious metals such as Zn have also been identified as possible candidates, although lower CO FE efficiencies are observed.[3−7] Ag catalysts are considered to be promising alternatives because of their high FE for CO (81.5% at −0.97 V vs RHE[3]) and a price lower than that for Au. Moreover, numerous studies reported that nanostructuring Ag surfaces (nanoporous materials,[8−10] nanocorals,[11] nanoplates,[12] nanosheets,[13] and nanoparticles[14]) can lead to a

decrease in the overpotential of up to a few hundred millivolts (mV), with efficiencies for CO reaching over 90%.

To further improve the catalytic activity, recent investigations have focused on oxide-derived metal catalysts[15] including Cu,[16] Au,[17] Sn,[18] and Pb.[19] In these systems, the total/partial reduction process of the preoxidized catalysts is thought to give rise to rougher surfaces with new active sites at grain boundaries as well as to residual cationic metal species or subsurface oxygen which might play a role in the catalytic selectivity. In the case of oxide-derived Ag catalysts, a fundamental understanding of the mechanisms leading to the decreased overpotential and increased CO selectivity is still needed.[20−23] For example, preoxidized Ag surfaces have been reported to display a stronger binding of reaction intermediates such as COOH* and CO*,[20] which was assigned to a high local pH. On the other hand, the superior catalytic activity and selectivity of oxygen-plasma-pretreated Ag catalysts (90% CO FE at −0.6 V vs RHE) were assigned to locally enhanced negative electric fields at defects created in the Ag surfaces by the plasma oxidation.[23] Unfortunately, the selectivity for the hydrogen evolution reaction (HER), a competing reaction against CO_2RR, was found to increase over time during the reaction as the original AgO_x films were reduced and the surface roughness decreased. Therefore, additional work is still required in order to develop Ag-based CO_2RR catalysts with

not only improved activity and C1-product selectivity but, more importantly, also enhanced stability.

Bimetallic systems have recently attracted attention as promising catalysts in order to achieve active but also stable CO_2RR. For instance, considerably enhanced FE toward C1 products[24,25] was obtained for systems consisting of noble metals (Au, Ag, or Cu) and nonprecious metals (Sn or In) mixtures by tuning the adsorption energy of intermediates.[6,26−28] Because Ag−Sn core−shell nanoparticle catalysts lead to ∼80% FE toward formate during 24 h of CO_2RR at −0.8 V vs RHE in 0.5 M $NaHCO_3$,[6] Ag-based bimetallic systems have been proposed as viable alternatives to maintaining stable C1-product selectivity.[29] In the case of Ag films, Larrazábal reported that indium deposited on a bulk Ag electrode (In@Ag) showed an enhanced CO current efficiency at moderate overpotential in comparison to bulk Ag.[24] However, the current efficiency for HER also increased up to 60% within 2 h of CO_2RR, coinciding with the change in chemical state of the In species. Despite the promising results obtained thus far on Ag films for CO_2RR, further efforts to suppress HER for long-term operation is still needed on the basis of the fundamental understanding of the parameters responsible for the distinct activity and selectivity of Ag-based CO_2RR catalysts.

Herein, we present a Ag-based catalyst for CO/formate production from CO_2RR displaying strongly suppressed HER (below 5% FE at −0.8 V vs RHE) during 20 h. The catalysts were synthesized by electrodepositing Sn on O_2-plasma preoxidized Ag films. Quasi *in situ* X-ray photoelectron spectroscopy (XPS), *operando* X-ray absorption near-edge structure spectroscopy (XANES), and *ex situ* scanning electron microscopy equipped with energy-dispersive X-ray spectroscopy (SEM-EDS) were employed to investigate the chemical state and surface morphology of the catalysts at different stages of the reaction in order to extract correlations among the structure, chemical state, and composition of the electrocatalysts and their activity and selectivity.

2. EXPERIMENTAL DETALS

2.1. Catalyst Synthesis. For the synthesis of Ag-based catalysts, Ag foils (99.97% purity and 125 μm thickness) were mechanically polished with silicon carbide paper (400 grit) and subsequently rinsed in deionized water and dried with argon (Ar). Oxygen plasma treatments (Plasma Prep III, SPI) were employed to modify the roughness and oxidation state of the Ag foils (denoted as AgO_x). The plasma conditions were 20 W and 350 mTorr O_2 for 2 min. To electrodeposit Sn on a metallic Ag surface (denoted as a SnO_x/Ag sample after air exposure) and on the plasma-oxidized AgO_x surfaces (denoted as a SnO_x/AgO_x sample after air exposure), a conventional three-electrode system was used with an Ag/AgCl (3 M KCl) reference electrode and Pt mesh as the counter electrode. Electrochemical sequences with two steps consisting of linear sweep voltammetry (−0.75 V to −2.0 vs Ag/AgCl) with a sweep speed of 100 mV/s and chronoamperometry at −2.0 V vs Ag/AgCl for 1 min were employed in order to avoid the parallel deposition of impurities such as metal salts in the aqueous solution. A solution of 0.05 M $SnCl_2$ (98% and Alfa-Aesar) mixed with 2 M NaOH (99.3% and VRW Chemicals) was used for the electrochemical Sn deposition. The electrodeposited catalysts were washed with deionized water and subsequently dried with Ar gas.

2.2. Characterization. The morphology and chemical state of the catalysts were investigated by SEM with an FEI Quanta 200 FEG microscope and a liquid-N_2 EDS detector. The quasi *in situ* XPS measurements were performed in an ultrahigh-vacuum setup equipped with a Phoibos100 (SPECS GmbH) analyzer (pass energy, E_{pass} = 13 eV) and an Al anode of a XR50 (SPECS GmbH) X-ray source (P_{source}= 300 W). The transfer from the electrochemical cell toward the UHV system is done under a pressurized argon atmosphere (99.999% Ar). All XPS measurements were acquired at high resolution (0.05 eV) and correspond to an average of at least five scans. The Casa XPS software was used for data analysis. All spectra were aligned to the C 1s region (E_b = 284.8 eV). The presented fits of the XPS spectra where made by first measuring the corresponding bulk references. SnO, SnO_2, Ag_2O, and AgO powders (99.999% Sigma-Aldrich) were measured as references for the different oxides, and Ar-sputtered (UHV-treated) Sn and Ag foils were used as references for the metallic spectra. All reference spectra used for fitting were additionally constrained with respect to their energy position (dE = 0.05 eV), using the corresponding values reported in the literature.[30,31]

To evaluate the catalytic performance, a home-built H-type electrochemical cell separated by a Selemion anion exchange membrane was used for CO_2 electrolysis at room temperature with an AutoLab PGSTAT128N potentiostat. A Pt mesh was used as the counter electrode, and a leak-free Ag/AgCl electrode (LF-1, Innovative Instruments, Inc.) was used as the reference. CO_2RR was carried out in a purified 0.1 M $KHCO_3$ solution by applying a potential between −0.6 and −0.8 V vs RHE under a constant 20 mL/min CO_2 flow rate. Prior to the electrochemical reaction, the electrolyte was purified with Chelex 100 Resin (Bio-Rad)[32,33] in order to minimize the effect of metal impurities in the electrolyte and subsequently purged with CO_2 gas (99.95%) for 30 min to reach a pH value of 6.8. The gas products were injected into an online gas chromatograph (Agilent 7890A) every 17 min during CO_2RR. Liquid products such as formate were detected by high-performance liquid chromatography (HPLC, Shimadzu) after CO_2RR. The value of the solution resistance was measured with the *iR* interrupt method[34] and electrochemical impedance spectroscopy. To determine the roughness factor of the catalysts, the double-layer capacitance was measured between 0 and 0.25 V vs RHE after 1 and 20 h of reaction in 0.1 M $KHCO_3$ (Figure S1 and Table S1 in Supporting Information).

Operando XANES measurements were conducted with a home-built electrochemical cell using Pt mesh (MaTeck) and leak-free Ag/AgCl as counter and reference electrodes, respectively. The measurements were made in fluorescence mode using a planar implanted silicon (PIPS) detector at the P64 undulator beamline of the PETRA III synchrotron radiation facility.

3. RESULTS AND DISCUSSION

3.1. Morphological Characterization. To synthesize stable Ag−Sn CO_2RR catalysts, O_2-plasma treatments on Ag foils and subsequent Sn electrodeposition were employed. Figure 1 presents SEM images of SnO_x/Ag and SnO_x/AgO_x bimetallic catalysts as prepared (top row) and after 20 h of CO_2RR at −0.8 V vs RHE (bottom row). A comparison with a monometallic AgO_x catalyst is also included. An enhanced surface roughness is observed for all samples resulting from either the O_2-plasma pretreatment or the Sn electrodeposition. On the basis of the roughness factors extracted from electrochemical double-layer capacitance measurements, the roughness was found to increase in the order of AgO_x > SnO_x/AgO_x > SnO_x/Ag > metallic Ag foil (Figure S1 and Table S1).

A strong change in the morphology of the AgO_x (Figure 1d) and SnO_x/AgO_x (Figure 1e) samples occurs after 20 h of CO_2RR, while the surface of the SnO_x/Ag sample (Figure 1f) is only mildly altered under reduction reaction conditions. The SnO_x/AgO_x sample already shows a slight change in surface roughness after 1 h of reaction (Figure S2). Our EDS analysis shows that the entire surface of the Ag and AgO_x substrates was covered with Sn.

3.2. Chemical State/Surface Composition Characterization. To gain further information on the chemical state of
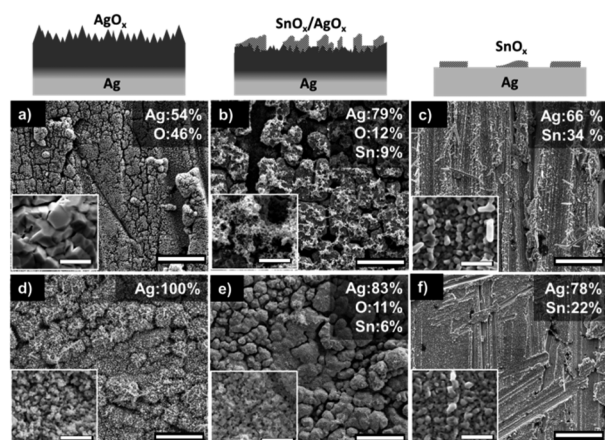
Figure 1. SEM images of AgO_x (a, d), SnO_x/AgO_x (b, e), and SnO_x/Ag (c, f) catalysts acquired before (a−c) and after CO_2RR at −0.8 V vs RHE for 20 h (d−f). The average values of the composition extracted from SEM-EDS measurements are also shown. The scale bars indicate 20 μm. The insets show higher-magnification images (scale bars, 2 μm).

the Ag−Sn bimetallic catalysts as prepared and after reaction, quasi *in situ* XPS measurements were carried out on the SnO_x/AgO_x and SnO_x/Ag samples before and after CO_2RR at −0.8 V versus RHE in an electrochemical cell directly attached to the XPS system.

As expected, after O_2-plasma treatment the Ag substrate is oxidized. (See the Ag MNN Auger spectra in Figure S3.) Nevertheless, after the *in situ* Sn electrodeposition, only metallic Ag is seen. This is directly linked to the strong reductive alkaline conditions employed during the Sn electrodeposition.[35] Moreover, it should be noted that the deposition process does not leave behind any residual Cl, which might influence the CO_2RR mechanism (Figures S4 and S6) by decreasing the overpotential for forming the CO_2 radical.[11]

By comparing the integrated area of the Ag 3d and Sn 3d XPS peaks (Figure S5), the Sn/Ag ratio on the surface of the SnO_x/AgO_x and SnO_x/Ag samples was 1:1 and 3:1 (Table S2), respectively. This ratio is higher than that extracted by EDX because Sn is deposited on top of the Ag substrates and XPS is a more surface-sensitive technique than EDX. Overall, the XPS data reveal that the catalyst surface composition is stable and that there is no evidence of sintering or interdiffusion of the two metals even after 20 h of CO_2RR.

Figure 2 displays Sn MNN Auger spectra from the SnO_x/AgO_x and SnO_x/Ag samples acquired as prepared and after 1 and 20 h of CO_2RR. In both samples, features corresponding to metallic Sn[31] are seen after the reaction, together with SnO_x species.[34] The progressive reduction of the SnO_x species is observed with increasing reaction time, but there are still Sn oxides present on the surfaces of both samples even after CO_2RR at −0.8 V vs RHE for 20 h (Figure 2 and Table S3).

Nonetheless, because of the quasi *in situ* nature of the former measurements and although the samples were never exposed to air during the transfer to the XPS chamber, they were still in contact with the electrolyte after reaction during the transfer (5−15 s) in the absence of an applied potential, which could result in partial reoxidation of the surface Sn species. To confirm that SnO_x species indeed remain stable under reaction conditions at the potentials of interest, *operando* X-ray absorption spectroscopy measurements were also conducted. XANES was used to gain insight into changes in the catalysts
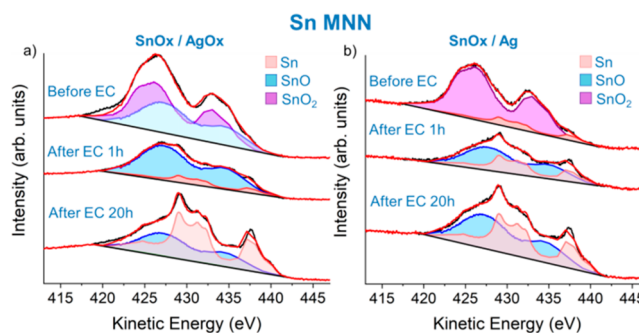
Figure 2. Quasi *in situ* Sn MNN Auger spectra of Sn electrodeposited on (a) an O_2-plasma-treated Ag substrate (AgO_x) and (b) a pristine Ag substrate. Colored spectra are Sn MNN reference spectra (metallic Sn, SnO, and SnO_2) used to fit the envelope of Auger spectra. Electrochemical CO_2RR has been performed at a working potential of −0.81 V vs RHE in 0.1 M $KHCO_3$.

chemical state and morphology during CO_2RR. It should be noted that this technique is bulk-sensitive, providing information from surface and subsurface sample regions. Furthermore, the fluorescence signal detected here is highly dominated by the radiation emitted by the silver support. Unfortunately, the Ag $K\beta$ emission line (24 941 eV) overlaps with the Sn $K\alpha$ series (24 735−25 272 eV), making the measurements of these samples at the Sn K edge very challenging. Nevertheless, insight into the chemical state of Sn before and under CO_2RR conditions can still be extracted by comparing to reference spectra (Figure 3).

The Sn spectrum of the SnO_x/Ag sample in Figure 3a resembles that of the Sn foil, showing a low-intensity feature above the edge (the so-called "white line") at 29 207.8 eV that barely changes under CO_2RR. This indicates that even though the sample surface might be oxidized, the signal of the metallic Sn subsurface layers dominates the XAFS spectrum. On the
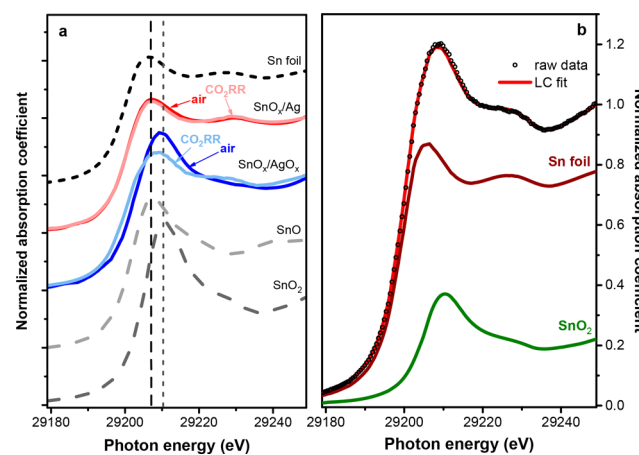
Figure 3. (a) Sn K-edge XANES spectra of Sn electrodeposited on O_2-plasma-treated Ag (SnO_x/AgO_x) and on a pristine Ag foil (SnO_x/Ag) measured as-prepared and under CO_2RR conditions after 5 h of activation at −0.8 V vs RHE in 0.1 M $KHCO_3$. Reference spectra of the metallic Sn foil, SnO, and SnO_2 are also shown. Vertical lines provide a guide for the eye and represent the white line position of the reference Sn foil, of bulk SnO (dashed line), and of bulk SnO_2 (dotted line). (b) Sn K-edge XANES spectrum of SnO_x/AgO_x (open circles) under CO_2RR conditions together with the linear combination fit (red solid line) and the weighted spectral components corresponding to Sn and SnO_2 species.

other hand, the sample deposited on plasma-treated Ag (SnO_x/AgO_x) is severely oxidized prior to the reaction as indicated by a more intense white line shifted to 29 209.6 eV. Under the reaction conditions, the white line gets broader but less intense and shifts to slightly lower photon energy. To get quantitative information on the Sn species observed, XANES spectra were fitted using a linear combination (LC) of the reference spectra of a Sn foil, SnO, and SnO_2 (Figure 3b). Because XANES spectra of both oxides show similar features and differ only in the intensity and position of the white line, an energy shift, fitted during linear combination analysis, served as an extra figure of merit along with the R factor. Thus, if two fits, using different oxides as principle components, resulted in similar R-factor values, then the one with a smaller energy shift was accepted. Hence, with these bulk-sensitive techniques, the as-prepared SnO_x/Ag sample was found to consist of 90% metallic Sn and a 10% mixture of SnO and SnO_2 in a 2:1 ratio. (See Table S4 and Figure S7 for details.) The LC analysis proves the full reduction of Sn in this sample under the reaction conditions. The SnO_x/AgO_x sample shows more severe oxidation in its as-prepared state, with Sn^0 and Sn^{4+} species present in a ratio close to 1:1. In contrast to the sample supported on pristine Ag, the SnO_x layer deposited on AgO_x was not fully reduced after 5 h under CO_2RR conditions with 23% of Sn remaining as SnO_2.

The combined results from XPS (surface-sensitive) and XANES (bulk-dominated) analysis indicate that although the surfaces of the SnO_x/Ag and SnO_x/AgO_x samples are oxidized in their as-prepared states, the oxide layer thickness is not very thick in the case of the SnO_x/Ag sample. This is concluded on the basis of the XANES data revealing a mainly reduced sample before and during CO_2RR, while only via the more sensitive XPS technique can one detect the partial reduction of the SnO_x species during the first 20 h of CO_2RR. On the other hand, SnO_x species were found to remain in the SnO_x/AgO_x sample not only at the surface (XPS) but also at the subsurface (XANES) at least within the first 5 h of the reaction.

3.3. CO_2RR Performance. Figure 4a shows the selectivity of electrocatalysts toward the main products such as CO, H_2, and formate at −0.8 V vs RHE in 0.1 M $KHCO_3$ after 1 h of CO_2RR. By utilizing a plasma-oxidized Ag foil as substrate, AgO_x and SnO_x/AgO_x catalysts show outstanding selectivity toward C1 products (~95% FE) versus the parasitic HER (<5% FE), whereas the SnO_x/Ag catalyst employing a metallic Ag foil as a support shows a higher FE for HER (30% after 1 h of CO_2RR) than on the AgO_x substrates.

A correlation is also found between the roughness and the catalytic activity, with enhanced activity for the rougher surfaces. The O_2-plasma treatment, resulting in rough and defect-rich AgO_x and SnO_x/AgO_x surfaces,[23] leads to 2-fold-enhanced catalytic activity as compared to that of analogous but flatter surfaces such as metallic Ag and SnO_x/Ag, as shown in Figure 4b. Nevertheless, for samples with similar roughness factors (AgO_x and SnO_x/AgO_x, see Table S1), the product selectivity is strongly affected by the presence of Sn, with the SnO_x/AgO_x sample producing more formate than the AgO_x sample but also generating less H_2 when the performance is evaluated over a longer period of time (20 h) (Figure 5).

Although CO_2RR catalysts based on plasma-oxidized Ag substrates display remarkable catalytic activity and selectivity for CO during the first hour of reaction, it is still essential to design stable catalysts that can suppress HER while maintaining the selectivity for C1 products. As can be seen
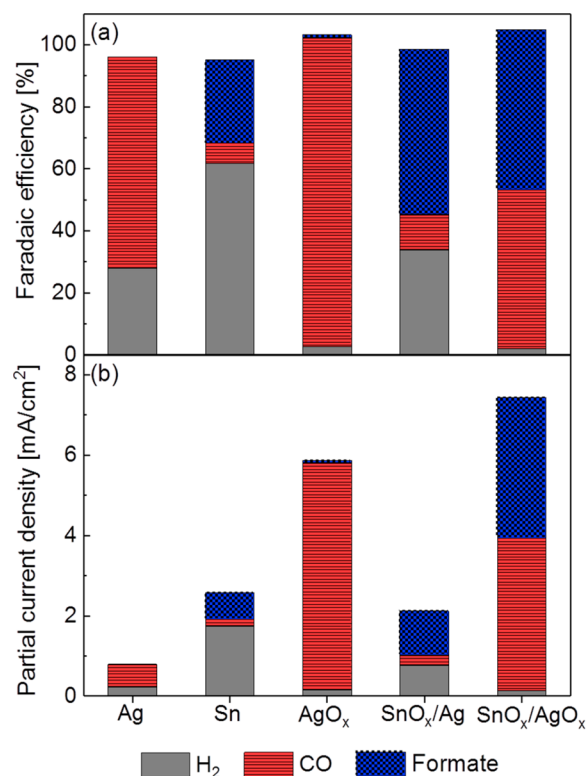

Figure 4. (a) Faradaic efficiencies and (b) partial current densities of AgO_x, SnO_x/AgO_x, SnO_x/Ag, metallic Ag, and Sn catalysts acquired after 1 h of CO_2RR at −0.8 V vs RHE in 0.1 M $KHCO_3$. Each column represents Formate (dotted blue), CO (straight red line), and H_2 (gray).

in Figure 5a, the monometallic AgO_x catalyst shows a distinct deactivation over time, with an increase in the HER pathway likely due to the decrease in the population of defect sites and the overall decrease in surface roughness with time.[23]

In contrast, the SnO_x/AgO_x sample is found to be significantly more stable in terms of the total current density and the C1 product conversion while maintaining a constantly low (5%) FE for H_2 (Figure 5b). A possible explanation for the stability of the SnO_x/AgO_x sample is that Sn electrodeposition on the rough AgO_x surface is able to preserve the surface roughness under reaction conditions better than when the AgO_x surface is uncoated. In fact, according to the roughness factors measured after different reaction times (Table S1), the roughness of the SnO_x/AgO_x surface is slightly increased after 20 h of reaction, while a decrease in the roughness is found for the pure AgO_x, which leads to the loss of highly active defect sites needed for the conversion to C1 products. The increase in the surface roughness reported to occur for SnO_x surfaces with decreasing oxide layer thickness was previously associated with a shift in surface orientation during electrolytic reduction.[36]

Interestingly, the ratio of the selectivity of formate and CO on the SnO_x/AgO_x catalyst changed from 1:1 after the first hour of reaction (Figure 4) to 1:3 after 20 h of reaction (Figure 5b) in spite of sustaining ~95% selectivity for C1 products. This phenomenon can be explained by considering the expected changes in the SnO_x thickness[25] during CO_2RR.[36] For instance, in Cu/Sn core/shell structures, 1.8 nm tin oxide shells are selective to formate, whereas thinner (0.8 nm) oxide shells favor CO formation. The later was explained on the basis of the SnO_x surface strain leading to a decrease in the
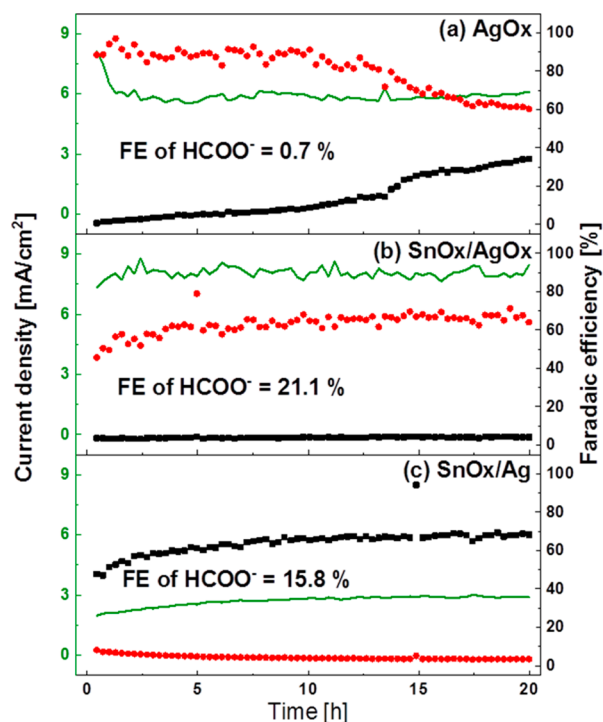
Figure 5. Temporal evolution of the activity and selectivity of different CO_2RR catalysts: (a) AgO_x, (b) SnO_x/AgO_x, and (c) SnO_x/Ag at -0.8 V vs RHE for 20 h during CO_2RR. Green lines indicate the total current densities (left y axis). Faradaic efficiencies (right y axis) of CO (red ●) and H_2 (■) are also shown. The FE value of $HCOO^-$ was obtained after 20 h of CO2RR.

overpotential forming intermediates.[25] Another plausible explanation for the temporal evolution of the CO and formate selectivity are morphological alterations (see in Figure 1b,e and Figure S2) on the sample surface taking place during electrocatalysis.

Furthermore, the chemical state of the Sn species deposited on the surface appears to be a particularly important factor in determining the reaction selectivity. An electrode consisting of both Sn^0 and $Sn^{\delta+}$ ($\delta = 2, 4$) species has shown remarkable catalytic activity and FE toward formate compared to a native SnO_x or a fresh Sn^0 surface.[18] By employing *in situ* spectroscopic analysis (XPS and XANES), it is confirmed that these oxides at least partially survive under CO_2 reduction conditions[37,38] or are present as surface hydroxides in the divalent oxidation state, which has been suggested to play a key role in formate production over SnO_x thin film electrodes.[39] In summary, the enhanced catalytic selectivity for C1 products is assigned to the stabilization of cationic Sn species on the SnO_x/AgO_x samples while maintaining adequate roughness during long-term CO_2RR.

4. CONCLUSIONS

Ag−Sn bimetallic catalysts synthesized via Sn electrodeposition on O_2-plasma-pretreated Ag foils (SnO_x/AgO_x) were found to display enhanced C1 product selectivity ($\geq$95% at -0.8 V vs RHE) during CO_2RR while maintaining low HER (<5% after 20 h). In clear contrast, a nearly 40% increase in HER selectivity was obtained for Sn-free AgO_x during the same period of time. *Ex situ* SEM showed that the O_2-plasma treatment provided a highly roughened surface, while quasi *in situ* XPS and *operando* XANES data revealed the presence of

cationic Sn species stabilized at the SnO_x/AgO_x surface even after prolonged reaction times. Furthermore, such species are found to be much less stable at the SnO_x/Ag surface. We expect that the findings presented here on the important synergistic interplay between surface roughness and stable $Sn^{\delta+}/Sn$ species can further guide the rational design of more stable and efficient CO_2 electrocatalysts.

■ ASSOCIATED CONTENT

Ⓢ Supporting Information

The Supporting Information is available free of charge on the ACS Publications website at DOI: 10.1021/jacs.8b12766.

> Experimental procedures, SEM, quasi *in situ* XPS, *operando* XANES, and the determination of the surface roughness factors (PDF)

■ AUTHOR INFORMATION

Corresponding Author

*roldan@fhi-berlin.mpg.de.

ORCID

Beatriz Roldan Cuenya: 0000-0002-8025-307X

Notes

The authors declare no competing financial interest.

■ ACKNOWLEDGMENTS

■ REFERENCES

(1) Verma, S.; Kim, B.; Jhong, H.-R. M.; Ma, S.; Kenis, P. J. A. A Gross-Margin Model for Defining Technoeconomic Benchmarks in the Electroreduction of CO2. *ChemSusChem* **2016**, *9* (15), 1972−1979.

(2) Lee, S.; Park, G.; Lee, J. Importance of Ag−Cu Biphasic Boundaries for Selective Electrochemical Reduction of CO2 to Ethanol. *ACS Catal.* **2017**, *7* (12), 8594−8604.

(3) Kuhl, K. P.; Hatsukade, T.; Cave, E. R.; Abram, D. N.; Kibsgaard, J.; Jaramillo, T. F. Electrocatalytic Conversion of Carbon Dioxide to Methane and Methanol on Transition Metal Surfaces. *J. Am. Chem. Soc.* **2014**, *136* (40), 14107−14113.

(4) Rosen, J.; Hutchings, G. S.; Lu, Q.; Forest, R. V.; Moore, A.; Jiao, F. Electrodeposited Zn Dendrites with Enhanced CO Selectivity for Electrocatalytic CO2 Reduction. *ACS Catal.* **2015**, *5* (8), 4586−4591.

(5) Won, D. H.; Shin, H.; Koh, J.; Chung, J.; Lee, H. S.; Kim, H.; Woo, S. I. Highly Efficient, Selective, and Stable CO2 Electroreduction on a Hexagonal Zn Catalyst. *Angew. Chem., Int. Ed.* **2016**, *55* (32), 9297−9300.

(6) Luc, W.; Collins, C.; Wang, S.; Xin, H.; He, K.; Kang, Y.; Jiao, F. Ag−Sn Bimetallic Catalyst with a Core−Shell Structure for CO2 Reduction. *J. Am. Chem. Soc.* **2017**, *139* (5), 1885−1893.

(7) Jeon, H. S.; Sinev, I.; Scholten, F.; Divins, N. J.; Zegkinoglou, I.; Pielsticker, L.; Cuenya, B. R. Operando Evolution of the Structure and Oxidation State of Size-Controlled Zn Nanoparticles during CO2 Electroreduction. *J. Am. Chem. Soc.* **2018**, *140* (30), 9383−9386.

(8) Lu, Q.; Rosen, J.; Zhou, Y.; Hutchings, G. S.; Kimmel, Y. C.; Chen, J. G.; Jiao, F. A Selective and Efficient Electrocatalyst for Carbon Dioxide Reduction. *Nat. Commun.* **2014**, *5*, 3242.

(9) Rosen, J.; Hutchings, G. S.; Lu, Q.; Rivera, S.; Zhou, Y.; Vlachos, D. G.; Jiao, F. Mechanistic Insights into the Electrochemical

Reduction of CO2 to CO on Nanostructured Ag Surfaces. *ACS Catal.* **2015**, *5* (7), 4293−4299.

(10) Sun, K.; Wu, L.; Qin, W.; Zhou, J.; Hu, Y.; Jiang, Z.; Shen, B.; Wang, Z. Enhanced Electrochemical Reduction of CO2 to CO on Ag Electrocatalysts with Increased Unoccupied Density of States. *J. Mater. Chem. A* **2016**, *4* (32), 12616−12623.

(11) Hsieh, Y.-C.; Senanayake, S. D.; Zhang, Y.; Xu, W.; Polyansky, D. E. Effect of Chloride Anions on the Synthesis and Enhanced Catalytic Activity of Silver Nanocoral Electrodes for CO2 Electro-reduction. *ACS Catal.* **2015**, *5* (9), 5349−5356.

(12) Liu, S.; Tao, H.; Zeng, L.; Liu, Q.; Xu, Z.; Liu, Q.; Luo, J.-L. Shape-Dependent Electrocatalytic Reduction of CO2 to CO on Triangular Silver Nanoplates. *J. Am. Chem. Soc.* **2017**, *139* (6), 2160−2163.

(13) Lee, C.-Y.; Zhao, Y.; Wang, C.; Mitchell, D. R. G.; Wallace, G. G. Rapid Formation of Self-Organised Ag Nanosheets with High Efficiency and Selectivity in CO2 Electroreduction to CO. *Sustain. Energy Fuels* **2017**, *1* (5), 1023−1027.

(14) Kim, C.; Jeon, H. S.; Eom, T.; Jee, M. S.; Kim, H.; Friend, C. M.; Min, B. K.; Hwang, Y. J. Achieving Selective and Efficient Electrocatalytic Activity for CO2 Reduction Using Immobilized Silver Nanoparticles. *J. Am. Chem. Soc.* **2015**, *137* (43), 13844−13850.

(15) Li, C. W.; Ciston, J.; Kanan, M. W. Electroreduction of Carbon Monoxide to Liquid Fuel on Oxide-Derived Nanocrystalline Copper. *Nature* **2014**, *508* (7497), 504−507.

(16) Li, C. W.; Kanan, M. W. CO2 Reduction at Low Overpotential on Cu Electrodes Resulting from the Reduction of Thick Cu 2O Films. *J. Am. Chem. Soc.* **2012**, *134* (17), 7231−7234.

(17) Chen, Y.; Li, C. W.; Kanan, M. W. Aqueous CO2 Reduction at Very Low Overpotential on Oxide-Derived Au Nanoparticles. *J. Am. Chem. Soc.* **2012**, *134* (49), 19969−19972.

(18) Chen, Y.; Kanan, M. W. Tin Oxide Dependence of the CO2 Reduction Efficiency on Tin Electrodes and Enhanced Activity for Tin/Tin Oxide Thin-Film Catalysts. *J. Am. Chem. Soc.* **2012**, *134* (4), 1986−1989.

(19) Lee, C. H.; Kanan, M. W. Controlling H + vs CO2 Reduction Selectivity on Pb Electrodes. *ACS Catal.* **2015**, *5* (1), 465−469.

(20) Ma, M.; Trześniewski, B. J.; Xie, J.; Smith, W. A. Selective and Efficient Reduction of Carbon Dioxide to Carbon Monoxide on Oxide-Derived Nanostructured Silver Electrocatalysts. *Angew. Chem., Int. Ed.* **2016**, *55* (33), 9748−9752.

(21) Jee, M. S.; Jeon, H. S.; Kim, C.; Lee, H.; Koh, J. H.; Cho, J.; Min, B. K.; Hwang, Y. J. Enhancement in Carbon Dioxide Activity and Stability on Nanostructured Silver Electrode and the Role of Oxygen. *Appl. Catal., B* **2016**, *180*, 372−378.

(22) Jee, M. S.; Kim, H.; Jeon, H. S.; Chae, K. H.; Cho, J.; Min, B. K.; Hwang, Y. J. Stable Surface Oxygen on Nanostructured Silver for Efficient CO2 Electroreduction. *Catal. Today* **2017**, *288*, 48−53.

(23) Mistry, H.; Choi, Y.-W.; Bagger, A.; Scholten, F.; Bonifacio, C. S.; Sinev, I.; Divins, N. J.; Zegkinoglou, I.; Jeon, H. S.; Kisslinger, K.; et al. Enhanced Carbon Dioxide Electroreduction to Carbon Monoxide over Defect-Rich Plasma-Activated Silver Catalysts. *Angew. Chem., Int. Ed.* **2017**, *56* (38), 11394−11398.

(24) Larrazábal, G. O.; Martín, A. J.; Mitchell, S.; Hauert, R.; Pérez-Ramírez, J. Synergistic Effects in Silver−indium Electrocatalysts for Carbon Dioxide Reduction. *J. Catal.* **2016**, *343*, 266−277.

(25) Li, Q.; Fu, J.; Zhu, W.; Chen, Z.; Shen, B.; Wu, L.; Xi, Z.; Wang, T.; Lu, G.; Zhu, J.; et al. Tuning Sn-Catalysis for Electrochemical Reduction of CO2 to CO via the Core/Shell Cu/SnO 2 Structure. *J. Am. Chem. Soc.* **2017**, *139* (12), 4290−4293.

(26) Larrazábal, G. O.; Martín, A. J.; Mitchell, S.; Hauert, R.; Pérez-Ramírez, J. Enhanced Reduction of CO2 to CO over Cu−In Electrocatalysts: Catalyst Evolution Is the Key. *ACS Catal.* **2016**, *6* (9), 6265−6274.

(27) Sarfraz, S.; Garcia-Esparza, A. T.; Jedidi, A.; Cavallo, L.; Takanabe, K. Cu-Sn Bimetallic Catalyst for Selective Aqueous Electroreduction of CO2 to CO. *ACS Catal.* **2016**, *6* (5), 2842−2851.

(28) Rasul, S.; Anjum, D. H.; Jedidi, A.; Minenkov, Y.; Cavallo, L.; Takanabe, K. A Highly Selective Copper-Indium Bimetallic Electro-

catalyst for the Electrochemical Reduction of Aqueous CO2 to CO. *Angew. Chem., Int. Ed.* **2015**, *54* (7), 2146−2150.

(29) Cai, Z.; Wu, Y.; Wu, Z.; Yin, L.; Weng, Z.; Zhong, Y.; Xu, W.; Sun, X.; Wang, H. Unlocking Bifunctional Electrocatalytic Activity for CO2 Reduction Reaction by Win-Win Metal−Oxide Cooperation. *ACS Energy Lett.* **2018**, *3* (11), 2816−2822.

(30) Hoflund, G. B.; Weaver, J. F.; Epling, W. S. AgO XPS Spectra Initial and Final State Effects in the ESCA Spectra of Cadmium and Silver Oxides. *Surf. Sci. Spectra J. Chem. Phys.* **1994**, *311* (96).

(31) Kövér, L.; Kovács, Z.; Sanjinés, R.; Moretti, G.; Cserny, I.; Margaritondo, G.; Pálinkás, J.; Adachi, H. Electronic Structure of Tin Oxides: High-resolution Study of XPS and Auger Spectra. *Surf. Interface Anal.* **1995**, *23* (7−8), 461−466.

(32) Hall, A. S.; Yoon, Y.; Wuttig, A.; Surendranath, Y. Mesostructure-Induced Selectivity in CO2 Reduction Catalysis. *J. Am. Chem. Soc.* **2015**, *137* (47), 14834−14837.

(33) Jeon, H. S.; Kunze, S.; Scholten, F.; Roldan Cuenya, B. Prism-Shaped Cu Nanocatalysts for Electrochemical CO2 Reduction to Ethylene. *ACS Catal.* **2018**, *8* (1), 531−535.

(34) Gao, D.; Scholten, F.; Roldan Cuenya, B. Improved CO2 Electroreduction Performance on Plasma-Activated Cu Catalysts via Electrolyte Design: Halide Effect. *ACS Catal.* **2017**, *7* (8), 5112−5120.

(35) Delahay, P.; Pourbaix, M.; van Rysselberghe, P. Potential-PH Diagram of Silver Construction of the Diagram-Its Applications to the Study of the Properties of the Metal, Its Compounds, and Its Corrosion. *J. Electrochem. Soc.* **1951**, *98* (2), 65−67.

(36) Feng, H.; Laverty, S. J.; Maguire, P.; Molloy, J.; Meenan, B. J. Electrochemically Reduced Polycrystalline Tin Oxide Thin Films. *J. Electrochem. Soc.* **1996**, *143* (6), 2048.

(37) Dutta, A.; Kuzume, A.; Rahaman, M.; Vesztergom, S.; Broekmann, P. Monitoring the Chemical State of Catalysts for CO2 Electroreduction: An In Operando Study. *ACS Catal.* **2015**, *5* (12), 7498−7502.

(38) Dutta, A.; Kuzume, A.; Kaliginedi, V.; Rahaman, M.; Sinev, I.; Ahmadi, M.; Roldán Cuenya, B.; Vesztergom, S.; Broekmann, P. Probing the Chemical State of Tin Oxide NP Catalysts during CO2 Electroreduction: A Complementary Operando Approach. *Nano Energy* **2018**, *53*, 828−840.

(39) Baruch, M. F.; Pander, J. E.; White, J. L.; Bocarsly, A. B. Mechanistic Insights into the Reduction of CO2 on Tin Electrodes Using in Situ ATR-IR Spectroscopy. *ACS Catal.* **2015**, *5* (5), 3148−3156.